The Monte Carlo Method: Versatility Unbounded in a Dynamic Computing World
Chattanooga, Tennessee, April 17-21, 2005, on CD-ROM, American Nuclear Society, LaGrange Park, IL (2005)

DOSE DISTRIBUTIONS FOR CINEANGIOGRAPHIC EXAMINATIONS OF CORONARY ARTERIES

Schlattl H and Zankl M
GSF-National Research Center for Environment and Health, Institute of Radiation Protection
Ingolstädter Landstr. 1, 85764 Neuherberg, Germany
helmut.schlattl@gsf.de; zankl@gsf.de

ABSTRACT

In recent years it became gradually common to use so-called voxel phantoms, which are based on tomographic image data of real persons, to compute doses from environmental or clinical radiation sources. A well established quantity is the mean organ dose, which is well suited for homogeneous and large irradiation fields. However, for smaller fields of weakly penetrating radiation steep dose gradients may occur in single organs, and the concept of mean organ dose does not provide sufficient information about the patient's actual radiation burden. We therefore modified our Monte Carlo code based on EGSnrc to record the dose not only for whole organs but for each voxel in a pre-defined area. As an example the spatial dose distributions for typical geometries used in cineangiographic examinations of the coronary arteries are computed. In addition, dose-volume histograms for the affected organs are determined. For this purpose, a female phantom was employed, which was segmented from CT data of an individual patient and then adjusted to reproduce total size, weight, and organ mass and volume from ICRP Publication 89. We found that, for instance, the dose in about 10% of the lungs may exceed the mean lung dose by a factor 5 and more.

Key Words: voxel models — EGSnrc — dose volume histograms — interventional radiology — angiography

1 INTRODUCTION

Ionizing radiation, naturally or man made, is a steady companion in human life. To assess its impact on human health the doses to organs or tissues are to be known. Since a direct measurement of these quantities is not possible, they are determined numerically employing simulations of the radiation transport in media. A basic ingredient in this computation is a virtual representation of the human body. In the past more or less simple geometrical objects have been used to represent the organ's shape. These so-called mathematical models have been partly outpaced by the development of so-called voxel phantoms based on real-patient computed or magnetic-resonance tomographic data. These phantoms consist of a large number of small volume elements (voxels) of the same size, but with different elemental composition and density according to the organ to which they belong. At GSF, for instance, a library of voxel phantoms has been built up, among which are models for baby, child and adults of various stature and weight [1].

With the help of these models, mean organ doses are computed to quantify the radiation risk of organs in various circumstances. However, for small fields of weakly penetrating radiation strong dose gradients can occur within single organs, such that mean organ doses provide only

limited information about the patient's radiation burden. For such cases, more detailed computations are required, where the spatial distribution of doses in organs is determined. We thus modified our existing Monte Carlo code (§2.1) to be able to perform this task.

A particular case, where large dose gradients may occur is the cineangiographic examination of the coronary arteries. There, only a small receptor plane of about 12 cm diameter is used with a focus-to-skin distance of about 50-60 cm. Therefore, the radiation is deposited only in a small fraction of large organs or tissues like lung and skin. We hence investigated one typical irradiation setup in this kind of examination; the results are summarized in §3. A brief description of the used Monte Carlo code and the irradiation energy spectra are provided in §2, where an analysis of the error estimate most suited for the resulting dose distributions is given, too.

2 COMPUTATIONAL MODEL

2.1 Monte Carlo Code

For the computation of the dose in voxel phantoms a user code developed at GSF is employed. It uses EGSnrc [2] for the particle transport and scoring of the energy depositions. In contrast to EGS4, the physics and the electron transport algorithm has been improved by the EGSnrc group [2]. In particular, bound Compton scattering and photo-electrons from K, L and M shell are included. For both effects, resulting fluorescence or Auger and Coster-Kronig electrons are taken into account. The electron collision stopping powers have been updated to the values recommended by ICRU 37 [3]. An enhanced multiple elastic scattering sampling routine including spin effects has been implemented as well as an improved transport algorithm, called Presta-II.

In the computations of this work the tracks of primary photons and secondary photons and electrons are followed down to kinetic energies of 1 keV. To compute the dose distributions the energy deposit of each particle is recorded not only for the individual organs but also in each voxel.

For the human phantom, a derivative of the voxel model LAURA of the GSF library [1] has been chosen. This phantom of an adult female has been segmented recently to serve as the basis for a voxel model of the adult female Reference Man according to ICRP Publication 89 [4]. The data set has been chosen from a variety of whole body CT scans of real patients, since the patient's external dimensions (height 167 cm, weight 59 kg) are close to the respective ICRP reference data (163 cm, 60 kg). Subsequently, the segmented voxel model has been modified to represent the ICRP adult female Reference Man concerning individual organ masses as well as total body height and weight. The resulting phantom is called KLARA, hereafter. A more detailed description is provided in Ref. [5].

In typical cineangiographic examinations of coronary arteries an X-ray tube about 50 to 60 cm from the skin with a receptor of about 12 cm diameter at a 90 cm distance is used. Three representative X-ray spectra were generated at GSF to match the beam quality used in cineangiography of female patients. They are characterized by half value layers (HVL) of 2.0, 3.5 and 5.0 mm Al, corresponding to peak tube potentials of 50, 80 and 110 kV. In Ref. [6] 11 different irradiation geometries have been evaluated to quantify the patient's risk. We computed

the dose distributions for almost all these geometries, where one of these has been depicted exemplarily for this work to show the distribution in detail.

2.2 Statistics

To obtain trustworthy results from statistical methods like Monte Carlo simulations it is essential to obtain reliable error estimates. Since for dose distributions the *number* of voxels with a dose in a certain interval is needed, a reliable error for the dose in each voxel is demanded. This can be seen, e.g, by comparing the differential dose volume histograms (DDVH) of the lungs for different numbers of particle histories (Fig. 1). The relative dose error in each voxel has been defined to be

$$\frac{\Delta D_i}{D_i} = \frac{1}{\sqrt{c_i}} \tag{1}$$

where D_i and c_i is the dose and the number of events in voxel i, respectively. This formula is exactly true, if the dose distribution in each voxel is an exponentially decaying one. We verified that for energies larger than about 80-100 keV this is a good approximation.

The total standard error in n_i, the number of voxels with doses within a certain dose interval i, is given by

$$\Delta n_i^{\mathrm{std}} = \sqrt{\sum_k (\Delta \eta_k)^2}, \tag{2}$$

where $\Delta\eta_k/\eta_k$, the relative number error of each voxel, has been taken to be equal to $\Delta D_i/D_i$, the relative error in the dose of each voxel. ($\eta_k = 1$ for each single voxel.)

In Fig. 1a the resulting DDVHs for the lungs with $32\ 10^6$ and $128\ 10^6$ particle histories and a geometry typical in cineangiographic examinations (Fig. 2) is shown. The incident photon spectra resembles an X-ray beam with HVL of 5.0 mm Al. All error bars have been obtained by Eq. 2. The red line denotes the case with $32\ 10^6$ histories, when all voxels with at least 2 events have been taken into account. They contain about 98% of the total dose to the lungs. For comparison, the $128\ 10^6$ history case is represented by the black histogram.

The errors are small even for low dose bins ($D_i/\langle D\rangle \leq 0.3$), but the histograms do not overlap. Even on a 3σ level they would hardly be in agreement. Considering the number of events in each voxel for these low dose bins in the $32\ 10^6$ histories case, their small value is noticed. The green histogram in Fig 1a shows the results, if only those voxels with event numbers larger than 10 are taken into account. Obviously, a large number of voxels do have a very low event number and thus “bad” statistics. But due to the large number of those voxels, the formal standard error for low-dose bins remains small. Note, that the relative standard error scales with $1/\sqrt{n_i}$.

A better error estimate can be obtained by using the maximal, instead of standard error:

$$\Delta n_i^{\max} = \sum_k |\Delta \eta_k|. \tag{3}$$

Here the error does not scale with $1/\sqrt{n_i}$ but is the mean of the individual errors in each bin. In Fig. 1b the resulting error bars using this definition are shown. They are considerably larger and, in particular, in the low-dose bins the results from $32\ 10^6$ and $128\ 10^6$ histories are in

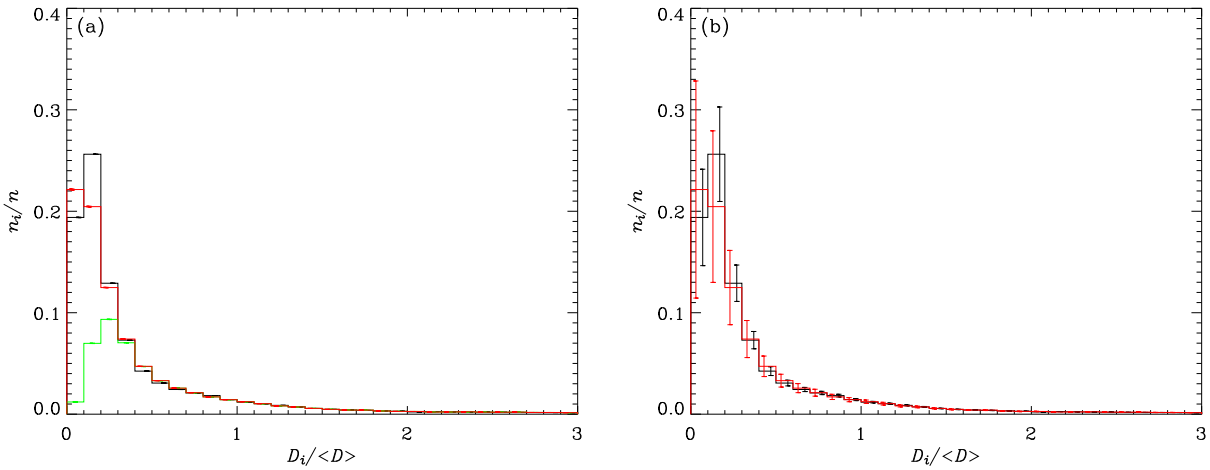

Figure 1: a) Comparison of differential dose volume histograms for the lungs irradiated with an X-ray beam with HVL of 5.0 mm Al using $128\ 10^6$ (black line) and $32\ 10^6$ (red) particle histories, where n_i is the number of voxels within the dose interval *i*. *n* and $\langle D \rangle$ are the total number of voxels and the mean dose of the lungs, respectively. In both cases, only those voxels have been counted with more than 2 events. For comparison, the green line represents the $32\ 10^6$ history case where all voxels with at least 10 events are considered. The error bars correspond to the statistical error (Eq. 2).
b) as a) but showing the maximal errors $\Delta n_i^{\max}$ (Eq. 3).

agreement. We therefore conclude, that a much more realistic error estimate is obtained using the maximal instead of standard error, and hence are using $\Delta n_i^{\max}$ in our evaluation.

In any case, for the high-dose bins, a history number of $32\ 10^6$ is sufficient. Therefore all computations for the dose and dose volume histograms, if not stated explicitly, are performed with this number.

3 RESULTS

KLARA has been irradiated with a photon point source with 3 energy spectra, which correspond to X-ray beams with 50, 80 and 110 kV tube potential and total filtration of 3.3, 3.9 and 4.2 mm Al, resulting in HVLs of 2.5, 3.5 and 5.0 mm Al, respectively. The geometry is shown in Fig.2, where the source-to-skin and the source-to-image-receptor distance are 70 and 95 cm, respectively. The field-of-view diameter of the image receptor is 12 cm.

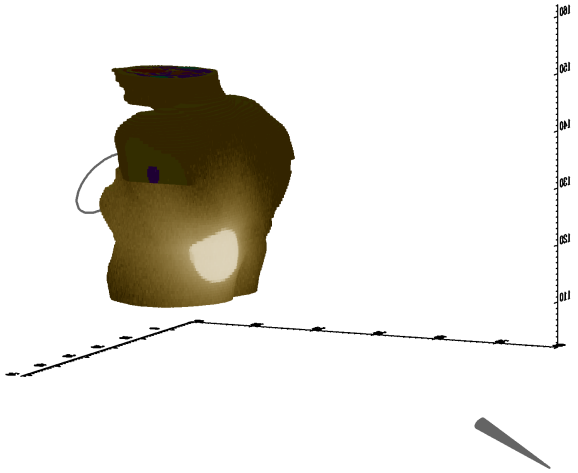

Figure 2: The irradiation geometry used for the cineangiographic examination investigated here. The source and X-ray beam are indicated by the small cone in the lower right corner, the field by the ring just behind the phantom's chest. Only that part of KLARA is shown, where the dose distribution is recorded. Note, that for this kind of examination, the patient usually has to lift his arms. Thus, they have been removed from KLARA. The brightness of the skin scales with the absorbed dose.

3.1 Organ Doses

The doses in KLARA's organs being mainly exposed to radiation by this examination geometry are summarized in Table I together with the values from the mathematical phantom EVA [6]. The differences in the organ doses are mostly of the order of 20-30%, but in some cases even up to a factor of 2. The basic reason is a different shape and location of the organs relative to the edge of the beam in KLARA and EVA. The most significant deviations can be observed for the spleen and the adrenals. While in EVA the adrenals are much more exposed and the spleen receives a dose almost an order of magnitude less, just the opposite is observed in KLARA.

The about 10% smaller dose of that part of the skin in KLARA, which is directly irradiated by the source, has been caused by the body shape, which is much simpler in EVA. We also have shown the maximum dose of the skin, which is about 15% larger than the mean dose in the

Table I: The tissue doses per 1 Gy air kerma (free-in-air at skin-entrance plane) for exposure geometry RAO 15° Cranial 25° centered on the left ventricle (Fig 2). The doses for EVA are from Ref. [6], where also more details about the geometry can be found. The rightmost column contains the largest coefficient of variance for KLARA.

HVL (mm Al)	2.5		3.5		5.0		Max.
Tissue	Dose (mGy/Gy)						CV
	EVA	KLARA	EVA	KLARA	EVA	KLARA	(%)
Entrance skin in primary field	959	884	1109	1018	1188	1086	0.09
Maximum dose in entrance skin	—	997	—	1169	—	1246	2.12
Brain	0.001	0.002	0.016	0.029	0.039	0.077	4.20
Thyroid	0.074	0.396	0.44	1.92	0.92	3.33	3.12
Thymus	2.4	1.36	9.5	5.39	16.5	9.34	1.55
Active bone marrow	5.4	4.44	11.9	9.94	17.4	14.3	0.04
Esophagus	11.6	14.3	34.6	35.1	54.6	50.5	0.37
Lungs	26.7	31.5	49.2	57.8	64.1	75.1	0.05
Breast	2.4	3.36	8.1	11.0	13.3	18.1	0.21
Heart	21.2	38.5	59.9	89.8	91.7	127.	0.05
Adrenals	66.8	7.24	125	20.2	163	30.1	0.80
Spleen	10.0	121.	25.7	210	36.5	265.	0.06
Pancreas	7.2	1.71	22.2	6.48	34.2	10.7	0.52
Stomach	2.4	18.8	8.8	42.7	14.4	59.6	0.15
Liver	0.78	2.48	3.9	9.02	7.0	14.9	0.12
Kidneys	3.5	4.90	9.6	12.8	14.2	18.7	0.19
Colon	0.055	0.057	0.39	0.332	0.81	0.673	1.70
Small intestine	0.067	0.730	0.49	2.48	1.00	4.00	0.30
Ovaries	0.004	0.008	0.085	0.023	0.21	0.105	25.85
Uterus	0.006	0.005	0.095	0.039	0.21	0.097	12.38
Urinary bladder	0.001	0.004	0.030	0.022	0.064	0.068	18.76

entrance skin. This should be taken into account when determining the probability of a tissue reaction that may occur for local skin doses above approximately 2 Gy.

3.2 Spatial Dose Distribution

The spatial dose distribution is displayed in Fig. 3. For this particular case, the number of histories used was $128\ 10^6$. The irradiated tissues can be seen clearly by the brighter regions. The isocontour lines give an overview of the absolute absorbed dose (in mGy/Gy). Apart from the main target of this examination, the heart, in particular, lung and spleen (brown, below horizontal plane) are exposed to the radiation, in agreement with the results for the mean organ doses (Table I). Remarkably is also the higher dose in bones compared to their surrounding tissue, which is caused by their higher absorption coefficient.

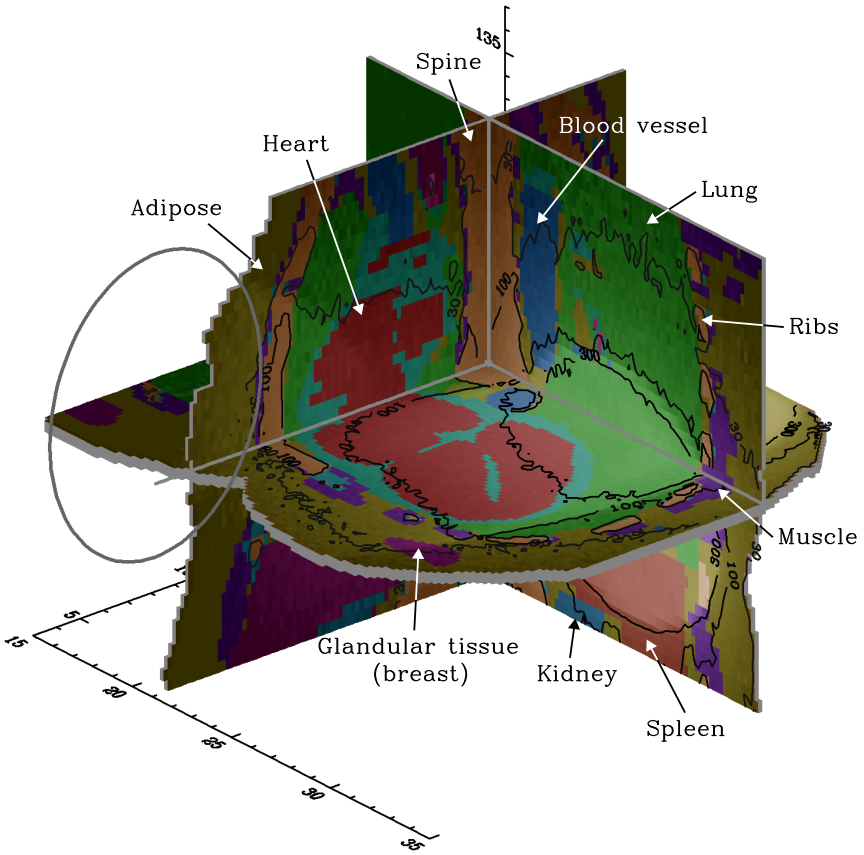

Figure 3: The spatial dose distribution in KLARA irradiated by photons with an energy spectrum corresponding to an HVL of 5.0 mm. The phantom is oriented such that the left anterior is in the foreground. The dose is represented by brightness and isocontour lines with values of 300, 100 and 30 mGy/Gy. The organs are color-coded as indicated. Note, that the heart consists of wall (turquoise) and content, i.e., blood (red). The image receptor plane is indicated by the circle in front of the chest.

3.3 Dose Volume Histograms

A more quantitative result is obtained by using dose volume histograms as in Fig. 4. The spread in the dose for the inner organs exposed in this examination varies from 3 to 15 times their mean dose values. In particular, for the lungs this might be relevant, as there about 10% of tissue gets 5 times more dose, and about 1% even 10 times more, than on average. Although the relative numbers may be low, it still means that about 10 g of the lungs is exposed to a dose of more than 300 mGy/Gy. Note, that the major radiation damage in this type of intervention has been observed on the entrance skin of the primary field, which amounts only to about 10 g and receives a dose of about 900 mGy/Gy.

The skin with its large extension compared to the irradiation field obviously shows the largest

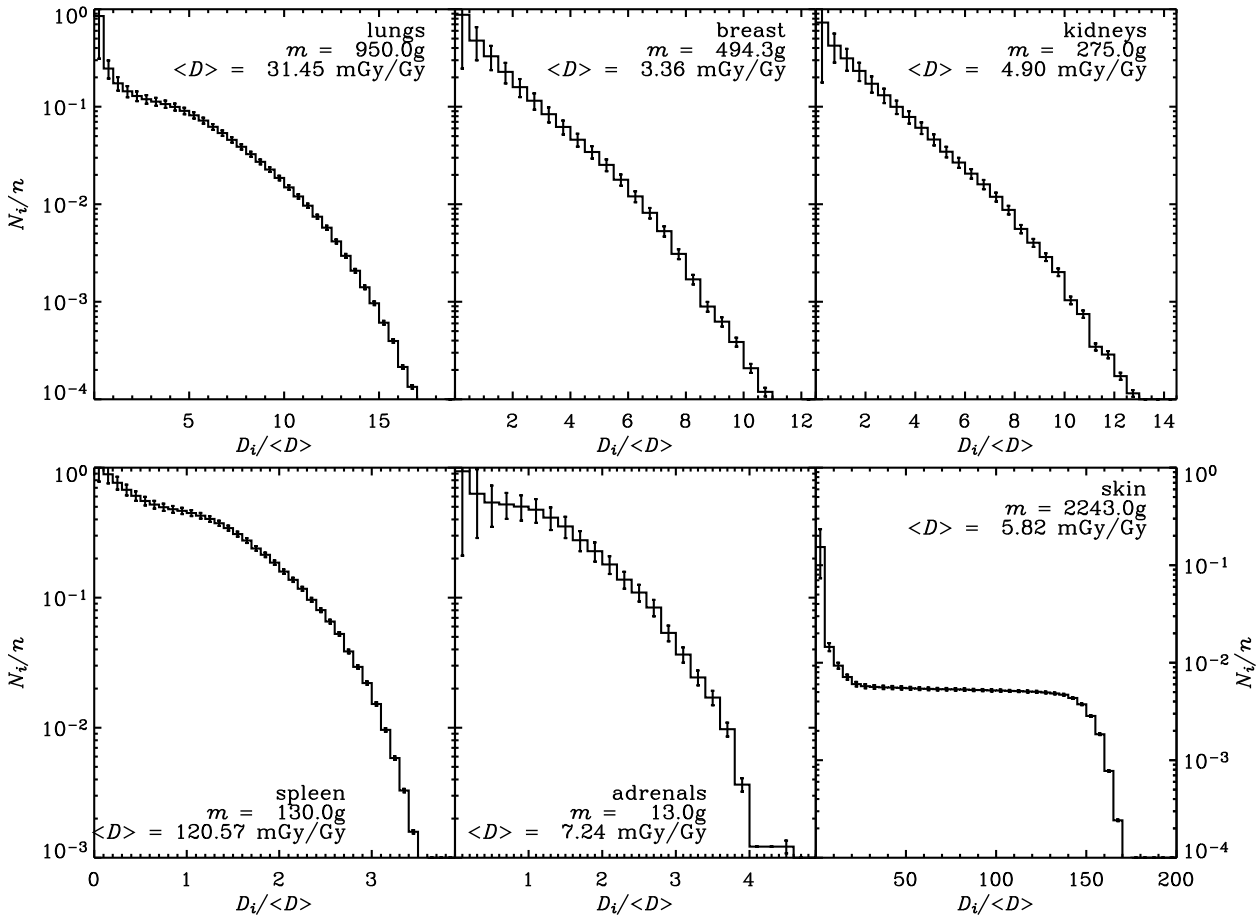

Figure 4: Dose volume histograms of selected organs for photon irradiation with an energy spectrum corresponding to an HVL of 2.5 mm (50 kV). For the ordinate the integrated number of voxels $\mathrm{N_i}$ is employed, where $\mathrm{N_i} = \sum_{\mathrm{k>i}} \mathrm{n_k}$.

spread in absorbed dose. As already mentioned, the high dose is received in the entrance skin, while at the exit skin the dose is only about 50 mGy/Gy. Observe, that in Fig. 4 the total number of skin voxels (i.e., the value at $D_i = 0$) is only $0.2\,n$, since the major part of the skin is outside the volume for which the spatial dose distribution has been recorded. This 80% of skin voxels contribute less than 2% to the mean absorbed dose of the skin.

4 CONCLUSIONS

The doses for cineangiographic examinations have been recomputed employing the phantom KLARA whose external dimensions and individual organ masses are close to the values recommended by ICRP Publication 89 [4]. For the one irradiation geometry investigated we found differences compared to the mathematical phantom EVA in many organ doses up to 30%. For the doses to spleen and adrenals we obtained the largest deviations of up to an order of magnitude, which are caused by different organ locations relative to the edge of the X-ray beam.

Furthermore, the dose volume histograms for a selected number of organs and dose distributions have been evaluated with our Monte Carlo code. We showed that about 10 g of lung tissue absorbs a dose of more than 300 mGy/Gy, which is an order of magnitude higher than the mean organ dose for the lungs. We therefore conclude, that for this kind of examinations with relatively small fields and strong dose gradients, the mean organ dose provides only a very rough estimate of the organ's radiation burden, and a more thorough analysis is important.

Nevertheless, for this intervention usually radiograms from various directions are made. Since different parts of an organ are exposed in irradiations from diverse directions, the overall variation of the dose from all radiograms is smaller than that from only one X-ray examination. Hence, combining the mean organ doses as found in Ref. [6] (or Table I) provides probably a good estimate also for that tissue, which is stronger burdened in a single X-ray examination. But one should keep in mind, that the absorbed dose in some parts of the organ may still be considerably higher. Further investigations are therefore needed. In addition, the usage of a male phantom is planned, which, like KLARA, has characteristics in agreement with ICRP Publication 89 [4].

5 ACKNOWLEDGMENTS

This work has been financially supported by the German Federal Office of Radiation Protection under contract no. StSch 4417.

6 REFERENCES

1. N. Petoussi-Henss, M. Zankl, U. Fill, D. Regulla, "The GSF family of voxel phantoms," *Phys. Med. Biol.*, **47**, pp. 89-106 (2002).
2. I. Kawrakow, D. W. O. Rogers, "The EGSnrc code system: Monte Carlo simulation of electron and photon transport," *National Research Council of Canada*, **PIRS-701**, http://www.sao.nrc.ca/inms/irs/EGSnrc/pirs701.pdf, (2003).
3. International Commission on Radiation Units and Measurements, *Stopping Powers for Electrons and Positrons* **ICRU Report 37**, Bethesda, Maryland, USA (1984).
4. International Commission on Radiological Protection, *Basic Anatomical and Physiological Data for Use in Radiological Protection: Reference Values,* **ICRP Publication 89**, Pergamon Press, Oxford, United Kingdom (2002).
5. M. Zankl, J. Becker, U. Fill, N. Petoussi-Henss, K. F. Eckerman, "GSF male and female adult voxel models representing ICRP Reference Man," *Americal Nuclear Society Topical Meeting in Monte Carlo*, Chattanooga, TN, April 17-21, 2005, (2005).
6. S. H. Stern, M. Rosenstein, L. Renaud, M. Zankl, "Handbook of selected tissue doses for fluoroscopic and cineangiographic examination of the coronary arteries (in SI Units)", U.S. Department of Health and Human Services, Food and Drug Administration, Center for Device and Radiological Health, *HHS Publication FDA*, **95-8288**, (1995).